

17AAG Treatment Accelerates Doxorubicin Induced Cellular Senescence: Hsp90 Interferes with Enforced Senescence of Tumor Cells

Upasana Sarangi, Khande Rao Paithankar, Jonnala Ujwal Kumar, Vaidyanathan Subramaniam and Amere Subbarao Sreedhar

CSIR Centre for Cellular and Molecular Biology, Uppal Road, Hyderabad 500 007, Andhra Pradesh, India.
Corresponding author email: assr@ccmb.res.in

Abstract: Hsp90 chaperone has been identified as an attractive pharmacological target to combat cancer. However, some metastatic tumors either fail to respond to Hsp90 inhibition or show recovery necessitating irreversible therapeutic strategies. In response to this enforced senescence has been proposed as an alternate strategy. Here, we demonstrate that inhibiting Hsp90 with 17AAG sensitizes human neuroblastoma to DNA damage response mediated cellular senescence. Among individual and combination drug treatments, 17AAG pre-treatment followed by doxorubicin treatment exhibited senescence-like characteristics such as increased nucleus to cytoplasm ratio, cell cycle arrest, SA- β -gal staining and the perpetual increase in SAHF. Doxorubicin induced senescence signaling was mediated by p53-p21^{CIP/WAF-1} and was accelerated in the absence of functional Hsp90. Sustained p16^{INK4a} and H3K4me3 expressions correlating with unaffected telomerase activation annulled replicative senescence and appraised stress induced senescence. Despite increases in [(ROS)i] and [(Ca²⁺)i], a concomitant increase in cellular antioxidant defense system suggested oxidation independent senescence activation. Sustained activation of survival (Akt) and proliferative (ERK1/2) kinases fosters robustness of cells. Invigorating senescent cells with growth factor or snooping with mTOR or PI3 kinase inhibitors compromised cell survival but not senescence. Intriguingly, senescence-associated secretory factors from the senescence cells manifested established senescence in neuroblastoma, which offers clinical advantage to our approach. Our study discusses tumor selective functions of Hsp90 and discusses irrefutable strategies of Hsp90 inhibition in anticancer treatments.

Keywords: Hsp90, senescence, neuroblastoma, 17AAG, doxorubicin

Drug Target Insights 2012:6 19–39

doi: [10.4137/DTI.S9943](https://doi.org/10.4137/DTI.S9943)

This article is available from <http://www.la-press.com>.

© the author(s), publisher and licensee Libertas Academica Ltd.

This is an open access article. Unrestricted non-commercial use is permitted provided the original work is properly cited.



Introduction

Heat shock proteins (Hsps) are implicated in evading stress induced cell death programming and in adaptive cellular responses to stress.¹ The Hsp90 chaperone functions are entangled with tumor progression identifying this protein as a cancer chaperone.² In support of this, the surface expression of Hsp90 in cancers of the human nervous system (NB69, SH-SY5Y, SK-N-SH) correlated with enhanced survival and proliferation, whose functional blockade with 17-allylamino-17-demethoxygeldanamycin (17AAG) or geldanamycin compromised cell survival.^{3–5} As an exception, the drug resistant and metastatic human neuroblastoma, IMR-32 failed to respond to 17AAG treatment⁶ despite Hsp90 being the central regulator of cell signaling.^{7,8} The non-responsiveness may relate to major regulatory mechanisms such as tumor suppression.

In addition to essential oncogenic kinase activation, inactivation of tumor suppressor mechanisms involving p53-p21^{CIP/WAF-1} and pRb-p16^{INK4a} are significantly implicated in cancer progression. Despite occurrence of mutations in p53 tumor suppressor gene in a large number of human tumors, neuroblastoma retains functional protein, and this could be the reason why inactivating mutations in p53 enhances chemotherapy induced cytotoxicity.⁹ The neuroblastoma also comprise constitutive p16^{INK4a} expression independent of Rb phosphorylation.¹⁰ The constitutive p16^{INK4a} expression was presumed to act against not only cytotoxic pathways but to bypass senescence programming. To circumvent chemotherapeutics induced non-selective cytotoxicity and to promote the therapeutic potential of pharmacological inhibitors of Hsp90 in metastatic tumors, several combination drug treatment strategies have been proposed.^{6–8} These combination treatments, however, suffer due to induced stress response mechanism, which may help in cell recovery and in making aggressive cancer phenotypes or affect bystander cells due to lack of tumor selectivity.

The DNA topoisomerase I inhibitor, doxorubicin has been shown to induce senescence-like phenotype in cells exposed to prolonged treatments. Subsequent to these findings, doxorubicin combination with Akt targeting was shown to be effective in Akt positive cells for cancer treatment.¹¹ Nevertheless, neuroblastoma cells possess altered PI3K-Akt-mTOR pathway

activation that correlates with poor prognosis¹² and do not respond to Akt destabilization even with 17AAG induced disassociation of Akt from Hsp90 binding.⁶ Considering the constraints associated with 17AAG response in IMR-32 neuroblastoma, we hypothesized that functional bereavement of Hsp90 status combining with doxorubicin may effectively combat cancer.

In the present study, we investigated the acceleration of pre-sensitizing effects of Hsp90 inhibition on doxorubicin induced cellular senescence. The acquired senescence phenotype was characterized by increased senescence associated β -galactosidase (SA- β -gal) activity and senescence associated heterochromatin foci (SAHF). Senescence obtained was neither associated with oxidative damage nor involving telomere shortening. Biochemical analyses suggested involvement of p53-p21^{CIP/WAF-1} pathways in senescence activation, which is independent of pRb-p16^{INK4a} pathway. Further, the senescence phenotype was resistant to growth stimulus and exhibited multidrug resistance. The secretory factors present in the conditioned medium can activate senescence-like phenotype in other human tumor cells. Our findings suggest that Hsp90 acts as a barrier to enforced senescence response in tumor cells.

Materials and Methods

Cell cultures, treatments and reagents

IMR-32, SRA01, and jurkat cells were from American Type Cell Culture. Cells were grown and maintained in DMEM containing 10% fetal bovine serum albumin in the presence of penicillin (100 U/mL), streptomycin (50 μ g/mL) and kanamycin (30 μ g/mL) at 37 °C in a humidified incubator with 5% CO₂ supply. For treatments, 2 × 10⁵ cells were grown on cover glass (22 × 22 mm, Fisher Scientific, USA) in a 6-well culture dish (nunc, Thermo Scientific, USA) and incubated in complete medium either with doxorubicin (Sigma-Aldrich, USA) or with 17AAG (InvivoGen, USA) at different time intervals. The effective drug concentrations were standardized by analyzing their ability to induce cytotoxicity in case of doxorubicin and to degrade 90% of Hsp90 client proteins in case of 17AAG. The concentration used throughout the manuscript for doxorubicin was 0.1 μ M and for 17AAG it was 2 μ M.



Cell based assays

Fluorescence activated cell sorting (FACS, FACSCalibur, Becton Dickinson, USA) analysis for DNA content was performed by staining cells with propidium iodide (50 $\mu\text{g}/\text{mL}$; Sigma-Aldrich, USA). To measure intracellular reactive oxygen species, [(ROS)i], cells were stained with CM-H₂DCFDA (5 μM ; Dojindo, Japan), to measure intracellular calcium, [(Ca²⁺)i], cells were stained with Fluo 3-AM (1 μM ; Dojindo, Japan), to measure a change in mitochondrial membrane potential ($\Delta\Psi_m$), cells were stained with JC1 (40 nM; Invitrogen, USA). After incubation for 20 min in the dark, cells were washed off the fluorophore three times with PBS and analyzed in MoFlow (Becton Dickinson, USA). Each experiment was repeated a minimum of three for reproducibility and statistical significance. The data were analyzed with BD Cell-Quest Pro v5.2 software.

Senescence associated β -galactosidase (SA- β -gal) staining

The phase-contrast images of cells were captured using Axiovert 200 microscope (20 \times magnification; Carl Zeiss, Germany). The SA- β -gal staining was performed as explained earlier¹³ and observed under the Axiovert 200 microscope (20 \times magnification).

Reverse Transcriptase Polymerase Chain Reaction (RT-PCR)

The RNA was isolated using TRIZOL (Sigma-Aldrich, USA) method. The first strand cDNA was prepared from 1 μg total RNA using Prime Script 1st strand cDNA synthesis kit (Takara Bio Inc., Japan). The gene specific cDNA amplifications were performed using qualitative PCR primers in a dual block PCR machine (DNA Engine; Bio-Rad, USA). The primers used were cell cycle regulators: *p21* (Accession no. NM_000389.3), sense, 5'-GGAGCTGGGCGC GGATTC-3', antisense, 5'-AGGCCCTCGCGC TTCCAG-3'; *p53* (Accession no. NM_000546.4), sense, 5'-TTGCGTTCGGGCTGGGAG-3', antisense, 5'-GCCGCCGGTGTAGGAGCT-3'; *p16* (Accession no. NM_000077.4), sense, 5'-ATTGAATTCATG GAGCCGGCGGCG-3', antisense, 5'-ATTGGA TCCATCGGGGATGTCTGAG-3'; Hsps: *hsp70* (Accession no. NM_005346.4), sense, 5'-CCA TGGTGCTGACCAAGATGAAG-3', antisense, 5'-TCGTCGATCGTCAGGATGGACAC-3';

hsp27 (Accession no. NM_001540.3), sense, 5'-TCCCTGGATGTCAACCACTTCG-3', antisense, 5'-GGGACAGGGAGGAGGAAACTTG-3'; *hsp90* (Accession no. NM_001017963.2), 5'-TCCGGTATGAAAGCT TGACAG-3', antisense, 5'-CTGGTC-CAGATGGGCTTTGTT-3'; GAPDH, (Accession no. NM_002046.3), 5'-TGA AGGTCGGTGTGAACG-GATTTG-3', antisense, 5'-TGATGGCATGGACTGTGGTCATGA-3'. Quantification of blots was performed using Image J software.

Immunoblot analyses

Cell lysates were prepared using HEPES lysis buffer (20 mM HEPES, 10 mM NaCl, 1.5 mM MgCl₂, 0.1% Triton X-100, pH 7.6), 20 μg total protein was run on 10% SDS-PAGE and was transferred on to nitrocellulose membrane. The primary antibodies, HRPO- and FITC-conjugated secondary antibodies were obtained from Santa Cruz Biotechnology Inc., (USA).

Laser Scanning Confocal Imaging Microscopy

Staining for mitochondria and actin was performed in cells with CMX-Ros (200 nM; Invitrogen, USA) and oregon green phalloidin (50 nM; Invitrogen, USA) respectively and nucleus was stained with DAPI (50 nM; VECTASHIELD, Vector Labs, USA) and observed under laser scanning confocal imaging microscope (Leica TCS SP5, Leica Microsystems, Germany). All immunofluorescence experiments were performed on cells grown on cover glasses, with p16, trimethyl histone (H3K4me3) and γ H2AX antibodies (Santa Cruz Biotechnology Inc., USA).

Rhodamine 123 (Rh123) efflux assay

Cells were incubated with Rh123 (1 μM ; Dojindo, Japan) and analyzed in the FACSCalibur. The Rh123 efflux ratio was calculated by dividing the mean channel number with cyclosporin A (CsA) and mean channel number with Rh123 alone.

Real-time polymerase chain reaction (real-time PCR)

The telomerase activity was measured by quantitative telomerase detection kit (US Biomax, USA). A standard real time PCR was run in Realplex Real-time PCR machine (Eppendorf Mastercycler ep gradient S, Germany) with the TSR oligonucleotide



and the telomerase activity was calculated from the standard curve.

Colony forming assay (CFA)

Cells were mixed with molten soft agar at 37 °C, poured over a base layer of agar and allowed to grow in complete medium with 5% CO₂ supply. After eight days, cells were stained with 0.1% crystal violet and observed under Axiovert 200 microscope in differential interference contrast microscope (DIC, 5× magnification). The colony size in micro meters was calculated from πr^2 and plotted.

Neo-vascularization assay

Cover glasses were pre-coated with matrigel (BD Biosciences, USA) for 45 min and cells were spread on matrigel, incubated with complete medium containing the drugs for 24 h and the tube or colony formation was observed under Axiovert 200 microscope in DIC (5× magnification).

siRNA knockdown of Hsp90

Hsp90 siRNA was designed using Invitrogen BLOCK-iT™ RNAi designer software from HSP90 cDNA (Accession No. NM_005348.2). The three siRNA used in the present study were, oligo1, 5'-GAA CAAA CAAGATCGAACTCT-3'; oligo2, 5'-GAGA GAGCT CATTCAAATTCATCA-3'; oligo3, 5'-ACTCTGG GAAAGAGCTGCATATTAA-3'. The siRNA was introduced into the cells using nanoparticle based X-fect transfection reagent (Clontech, USA).

Evaluation of conditioned medium (CM) for senescence promoting secretory factors (SASPs)

IMR-32 cells were 17AAG pre-treated for 24 h followed by doxorubicin for 5 days, and after confirming the SA- β -gal positive staining of cells, the CM was collected and used for subsequent experiments. The immortalized human lens epithelium (HLE) cells- SRA01 and human T-lymphocytes- jurkat (0.1×10^6 /mL) grown on cover glasses (18 × 18 mm, Fisher Scientific, USA) were replaced with CM and maintained at standard culture conditions. The cells were monitored every day under the microscope for typical senescence morphology. Cells that exhibited senescence like-phenotype were stained for β -galactosidase and observed under the microscope.

Statistical analyses

The data presented are mean \pm SEM of minimum three independent experiments. The significance was calculated by student's *t*-test (SigmaPlot 10.0) and a value minimum of $P < 0.05$ is considered significant.

Results

17AAG combination decreases doxorubicin induced senescence response

Senescent cell morphology is typically associated with increased nucleus to cytoplasm ratio with protracted cellular extensions and increased SA- β -gal staining.¹⁴ At first, various concentrations of drugs (17AAG- 0.5 μ M to 10 μ M or doxorubicin-0.1 μ M to 2.0 μ M) was examined for induced cytotoxicity. The optimum concentrations (0.1 μ M for doxorubicin and 2.0 μ M for 17AAG) were selected where we observed 90% client protein degradation for Hsp90 and minimal DNA damage response using doxorubicin. To determine whether SA- β -gal positive cells are induced by doxorubicin (0.1 μ M), 17AAG (2.0 μ M) or their combination treatment, cells were treated for 6-days, stained with X-gal and observed under the microscope. Doxorubicin treatment precisely increased SA- β -gal positive cells with extended cell morphology (35% \pm 5%, $P < 0.001$). The 17AAG treatment showed aspecific β -gal staining, which did not correlate with senescence morphology. Doxorubicin and 17AAG combination treatment decreased SA- β -gal positive cells (14% \pm 3% against 35% \pm 5% of doxorubicin), thus, suggested impaired senescence response on prolonged Hsp90 inhibition (Fig. 1A and 1A1, $P < 0.01$).

To understand the indistinctness in β -gal staining of cells between doxorubicin and 17AAG treatments, live cell morphology was examined under the microscope. Doxorubicin treatment resulted in extended cellular connections along with increased nucleus to cytoplasm ratio, however, 17AAG treatment showed loss of surface contact. In the combination treatment, a few cells were found still attached to the substratum even on 6-day long treatment (Suppl. Fig. 1A). The adherent cells thus can be related to only SA- β -gal positive cells. The differential senescence response to different drugs may be related to survival potential of cells on prolonged treatments. Investigating the DNA

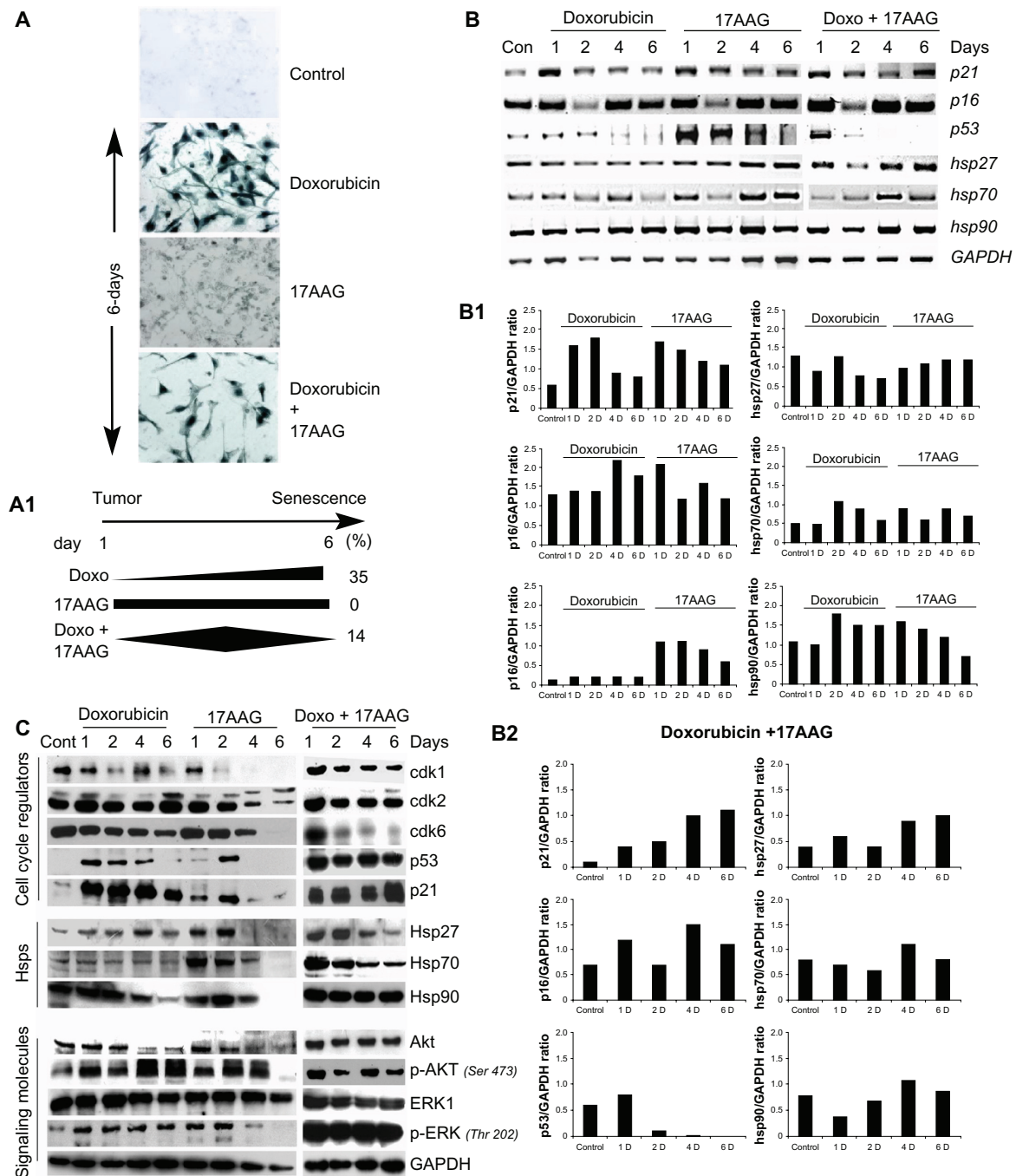


Figure 1. Effect of doxorubicin, 17AAG and their combination treatments on IMR-32 neuroblastoma cells. **(A)** SA- β -gal staining of control and 6-day drug treated cells. The images were captured at 20x magnification (Axiovert 200, Carl Zeiss). **(A1)** Statistical representation of individual and combination drug treatments induced percent SA- β -gal positive cells. **(B)** RT-PCR analysis of cell cycle regulators and heat shock genes on the onset of stress induced cellular senescence. **(B1 and B2)** Gene expression data was used to calculate the expression ratios in reference to GAPDH. **(C)** Immunoblot analysis of proteins from cell cycle, Hsps and signal transduction.

content of cells during the treatments by FACS analysis uncovered that doxorubicin and 17AAG treatments gradually increased subG1 population of cells. Interestingly, the combination treatment showed precipitous 50% increase ($P < 0.001$) in subG1 cells as early as in 3-days (Suppl. Fig. 1B).

17AAG and its combination with doxorubicin induces stress response
Tumor suppressors play a major role in deciding the fate of cells under stress conditions. To investigate their functional role in senescence, the expression levels of p21^{CIP/WAF-1}, p16^{INK4a} and p53 were examined by RT-PCR



analyses at 2-, 4- and 6-day post-treatments. The individual treatments showed a gradual decrease in p21^{CIP/WAF-1} along with the time of treatment. The combination treatment though showed an initial decrease in 2-day treatment, and a significant increase was observed by a 6-day treatment. Correlating with p21^{CIP/WAF-1} there was an increase in p53 expression in 17AAG (up to 4-day) and its combination with doxorubicin (by 1-day) corresponding to activation of cellular stress response. The doxorubicin induced p53, however, may be related to DNA damage response. Additionally, increased expression of stress proteins, Hsp27, Hsp70 and Hsp90 upon 17AAG and its combination with doxorubicin treatments further confirm activation of stress response (Fig. 1B). The ratio between each target gene and GAPDH expression was calculated using 'Image J' analysis to normalize loading controls and represented in bar diagram. Therefore the bar diagrams represent fold gene expression compared to GAPDH (Fig. 1B1 and Fig. 1B2).

To study protein levels of tumor suppressors, signal transduction and stress proteins, cell lysates collected at day 2, 4 and 6 of the treatments were examined by immunoblot analysis. Prolonged treatment of cells with individual drugs displayed gradual but radical decrease in cyclin dependent kinases, cdk1, cdk2 and cdk6, which has implications both in G1/S and G2/M cell cycle transitions. Prolonged combination treatment displayed a decrease in cdk6 alone that is involved in the G0 to G1 cell cycle transition. Doxorubicin and 17AAG treatments showed decrease in Hsp27, Hsp70 and Hsp90 levels; interestingly, only Hsp90 levels were unaffected by the combination treatment. Consistent with Hsp90 levels, Akt and ERK1/2 basal levels were not affected by the combination treatment compared to individual treatments. However, the phosphorylation status of Akt and ERK1/2 was found to be decreased (Fig. 1C).

17AAG pre-treatment but not the combination treatment accelerates senescence response

We excluded the combination treatments in our subsequent study, because prolonged treatments interfered with senescence activation by inducing early cytotoxicity (Suppl. Fig. 1B). In the following experiments, we studied pre-sensitizing effects of drugs on senescence acceleration. In brief, cells were treated with doxorubicin or 17AAG for 24 h and the drug

containing medium was replaced with fresh medium containing 17AAG or doxorubicin for 5-days were examined for SA- β -gal staining. Doxorubicin pre-treatment followed by 17AAG treatment showed fewer SA- β -gal positive cells (15% \pm 2%) by day-6 and 17AAG pre-treatment followed by doxorubicin treatment resulted in early (day-2, data not shown) SA- β -gal positive cells (65% \pm 11%) by day-6 (Fig. 2A and 2A1, $P < 0.001$). These results suggested that 17AAG pre-treatment accelerates doxorubicin induced cellular senescence, whereas, doxorubicin pre-treatment showed a response similar to doxorubicin treatment (compare Fig. 1A with Fig. 2A). In both the pre-treatments, SA- β -gal activity was correlating with typical senescence morphology (Suppl. Fig. 2A). However, doxorubicin pre-treatment resulted in enhanced cytotoxicity in comparison with 17AAG pre-treatment (Suppl. Fig. 2B). These findings establish that prolonged treatment of cells with 17AAG affects senescence activation. Further, a decrease in cytotoxicity (Fig. 2B, $P < 0.001$) in 17AAG pre-treatment was correlated with enhanced senescence (Fig. 2A), which is in agreement with the accumulation of cells in G1/S being a pre-requisite for senescence activation (14; Fig. 2C, $P < 0.001$).

17AAG pre-treatment retains survival potential

To investigate the difference in molecular mechanism of senescence activation in the pre-treatments, the RT-PCR analysis of cell cycle regulators was performed. A gradual decrease in p21^{CIP/WAF-1} in doxorubicin pre-treatment and a steady increase in 17AAG pre-treatment correlated with increased expression of p53 suggesting involvement of p53 and p21^{CIP/WAF-1} in senescence activation. The increased p21^{CIP/WAF-1} but not p16^{INK4a} expression correlated with enhanced SA- β -gal staining further suggested activation of stress induced cellular senescence. Increases in Hsp27, Hsp70 and Hsp90 levels in both the pre-treatments suggest induced synthesis or enhanced stabilization of their Hsp mRNA (Fig. 2D). Specific gene expression was calculated using Image J analysis in comparison with GAPDH to normalize loading controls and represented in bar diagram (Fig. 2D1).

Next, we examined protein profiles of regulatory molecules by immunoblot analysis using lysates of drug treated cells at days 2, 4 and 6. Though there

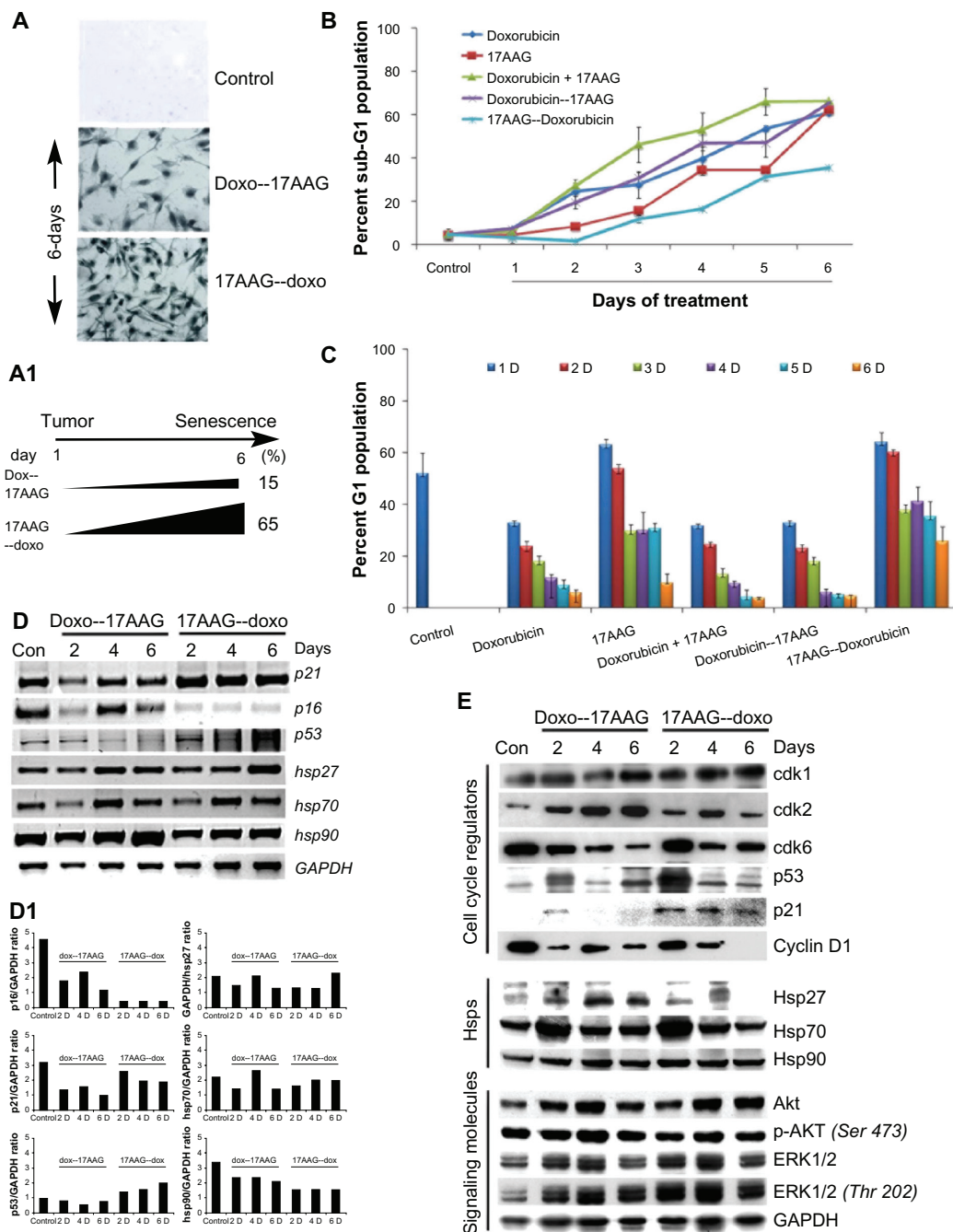


Figure 2. Effect of pre-treatments on IMR-32 neuroblastoma cells. **(A)** SA- β -gal staining of control and 6-day drug treated cells. **(A1)** Statistical representation of drug pre-treatment accelerated percent SA- β -gal positive cells. The images captured at 20x magnification (Axiovert 200, Carl Zeiss). **(B)** Percent cytotoxicity in individual, combination and followed drug treatments measured at 24 h time intervals for a period of 6-days. **(C)** Accumulation of G1 population after drug pre-treatments. **(D)** RT-PCR analysis of gene expression profiles after drug pre-treatments. **(D1)** Gene expression data was used to calculate the expression ratios in reference to GAPDH. **(E)** Immunoblot analysis of proteins from cell cycle, Hsps and signal transduction.

was some fluctuation in cdk1 levels, no significant change was observed both in doxorubicin pre-treatment or 17AAG pre-treatments suggesting no effect on mitosis. Increased cdk2 in doxorubicin pre-treatment suggested G1 clearing of cells but variability in 17AAG pre-treatment suggest crisis in

cellular decision making. The decrease in cdk6 levels in both the pre-treatments suggests inability of cells to re-enter cell cycle and can be argued with irreversible effects of cell cycle inhibition. While Hsp90 levels were unaffected by neither of pre-treatments, Hsp27 and Hsp70 levels showed an initial increase



in a 2-day treatment but its normalization by 6-day treatment. Correlating with increased levels of p53 and p21^{CIP/WAF-1}, a decrease in cyclin D1 levels suggested decreased proliferation potential. In contrast to individual and combination treatments, in the pre-treatments, a chronic activation of Akt and ERK1/2 kinases suggested maintenance of survival potential (Fig. 2E). Considering the accelerated senescence with 17AAG pre-treatment with reduced cytotoxicity, the subsequent experiments were performed with 17AAG pre-treatments.

17AAG pre-treatment shows typical features of senescence

Actin reorganization and nuclear accumulation was proposed as an additional marker for cellular senescence.¹⁵ To understand cellular actin dynamics, actin organization was examined in 17AAG pretreated senescent cells with Oregon Green Phalloidin. Compared to untreated cells, senescent cells showed a time dependent increase in peripheral actin bundling and accumulation of non-polymerized actin in the nucleus. Since sustained mitochondrial functions promote senescence activation,¹⁶ mitochondria organization was also examined with mitotracker red (CMX-Ros). Decreased actin bundling further correlating with increased mitochondria suggested conventional senescence activation (Fig. 3A). Increased intracellular granularity is considered as another characteristic feature of senescent cells,¹⁷ cells were analyzed for forward scatter (FSC) vs. side scatter (SSC) by FACS. We did not observe any change in FSC that provide information on particle size but observed a gradual increase in SSC that indicate increased intracellular granularity (Fig. 3B).

Accumulation of cells in G1 though suggested replicative senescence, involvement of p53- p21^{CIP/WAF-1} pathway highlighted stress induced senescence. To further distinguish the mode of senescence on 17AAG pre-treatment, telomerase activity was measured from senescent cells. A small increase in telomerase activity and its stabilization after 2-day treatment suggested cellular attempt to bypass senescence reprogramming (Fig. 3C), which is a characteristic feature of cancer cells.¹⁸ While H3K4me3 marks transcription start sites of active genes,¹⁹ senescence associated heterochromatin foci (SAHF) marks DNA damage response (DDR) to

senescence.²⁰ The cytoimmunofluorescence analyses of γ H₂AX (for SAHF) and H3K4me3 showed a gradual increase in SAHF but cytosolic accumulation of H3K4me3 (Fig. 3D and E respectively). Telomerase activity is linked to p16^{INK4a},²¹ however, neuroblastoma exhibit chronic p16^{INK4a} expression (Fig. 1B), which is thought to bypass senescence programming.²² To examine p16^{INK4a} cellular distribution, we performed cytoimmunofluorescence. Although, there was an increase in nuclear distribution in 2-day treatment, which has significantly decreased in 4- and 6-day treatments invalidating its role in senescence activation (Fig. 3F).

17AAG pre-treatment induced [(ROS)i] and [(Ca²⁺)i] promotes senescence and autophagy

Calcium permeation across membranes and mobilization from organelles was associated with senescence²³ along with increased [(ROS)i].²⁴ We measured [(Ca²⁺)i] and [(ROS)i] levels by FACS. In comparison with the control, we observed an initial increase in [(Ca²⁺)i] levels by 24.7 folds in 2-day treatment, which was decreased by 17.3 folds and 18.1 folds by day-4 and day-6 treatments (Fig. 4A, $P < 0.001$). There was also a gradual increase in [(ROS)i] levels by 2.6, 16.8 and 42.7 folds for day-2, -4 and -6 respectively (Fig. 4B, $P < 0.05$). Mitochondria being the major source of [(ROS)i] and the $\Delta\Psi_m$ is considered to be a biomarker for oxidative stress,²⁵ the $\Delta\Psi_m$ was measured by FACS. A gradual increase in negative polarization of mitochondria observed until 4-day time interval though suggested oxidative damage; a decrease by 6-day treatment suggests recovery from the oxidative stress (Fig. 4C, $P < 0.05$).

Since oxidative stress is caused by the imbalance between [(ROS)i] and impairment of antioxidative enzyme system,²⁶ we examined the status of antioxidative enzymes, superoxide dismutases, SOD1 (CuZn SOD, cytoplasmic), SOD2 (MnSOD, mitochondrial) and catalase (peroxisomes) in both doxorubicin and 17AAG pre-treatments by immunoblot analysis. The induced levels of SOD1, SOD2 and decreased levels of catalase on both the pre-treatments suggested activation of intracellular antioxidative defense, which also advocates non-lethal level production of [(ROS)i] (Fig. 4D). The gene expression analyzed by Image J and represented as gene

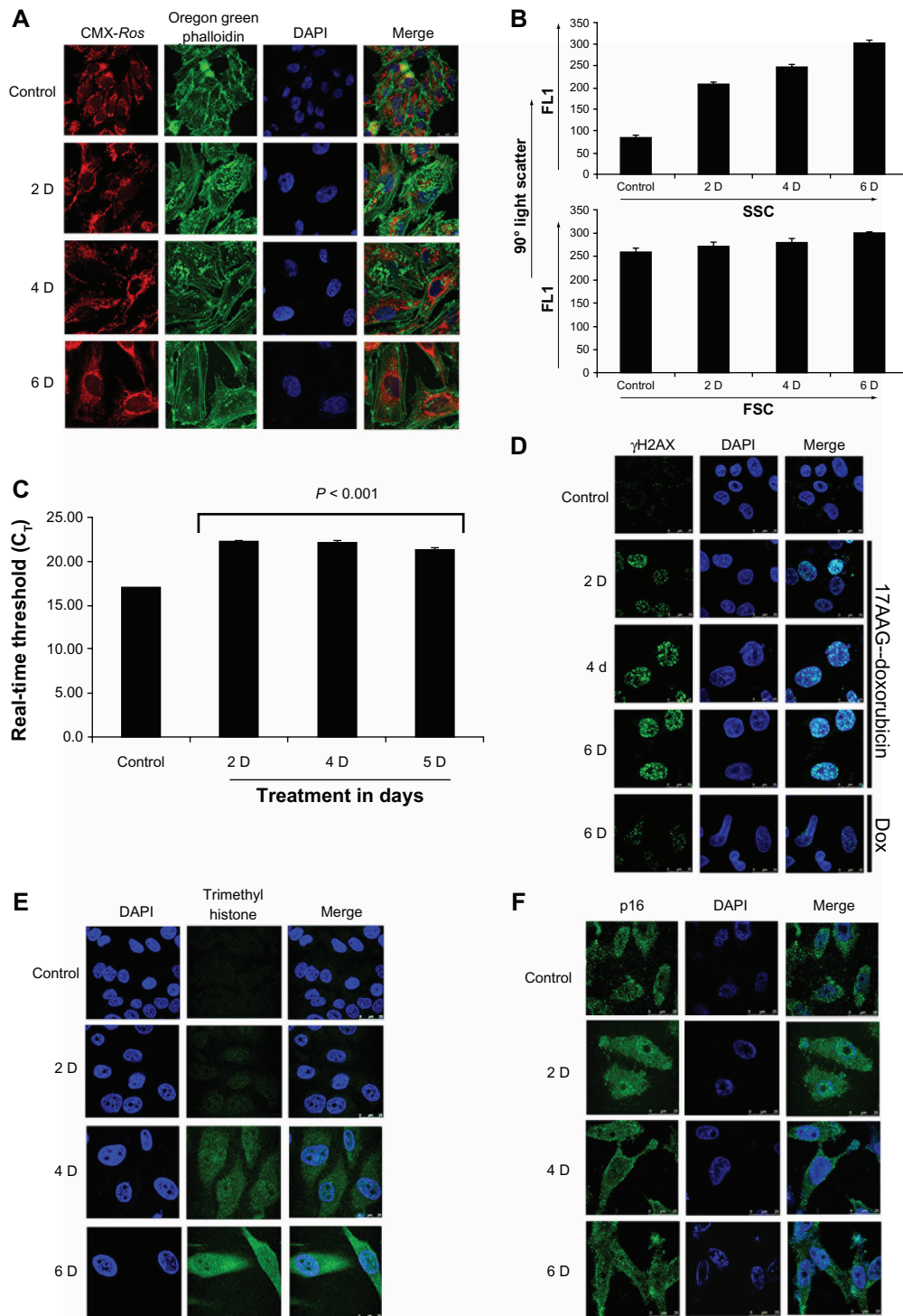


Figure 3. Molecular characterization of 17AAG pre-treatment accelerated cellular senescence. **(A)** Laser scanning confocal imaging microscope (Leica TCS SP5) analysis of cells stained with oregon green phalloidin (green) for actin, and CMX-Ros (red) for mitochondria. The nucleus was stained with 4', 6-diamidino-2-phenylindole (DAPI; blue). **(B)** 90 ° Light Scatter analysis by FACS. FL1 vs. SSC indicates granularity in the cells and FL1 vs. FSC indicates particle size inside the cells. **(C)** Real-time PCR analysis of telomerase activity. Real time threshold (C_t) was calculated from the kit standards and represented in bar diagram. **(D)** Cyto-immunofluorescence analysis of γ H₂AX for 17AAG pretreated cells for 2, 4 and 6-days. A 6-day doxorubicin treated cells were also presented for comparison. The secondary antibodies were conjugated to fluorescein isothiocyanate (FITC), therefore green color represents γ H₂AX. DAPI was used for nucleus staining. **(E)** Cyto-immunofluorescence analysis for H3K4me3 at 2, 4 and 6-day time intervals. Secondary antibodies were conjugated to FITC, hence green color represents H3K4me3. DAPI was used for nucleus staining. **(F)** Cyto-immunofluorescence analysis of p16^{INK-4a} at 2, 4 and 6-day time intervals. The secondary antibodies were conjugated to FITC. Nucleus was stained with DAPI. For all microscopy images, the scale bar represents 25 μ m at 100x magnification, The Z-section of each image was taken at 0.35 μ m intervals, and images represented are the merge of best Z-sections.

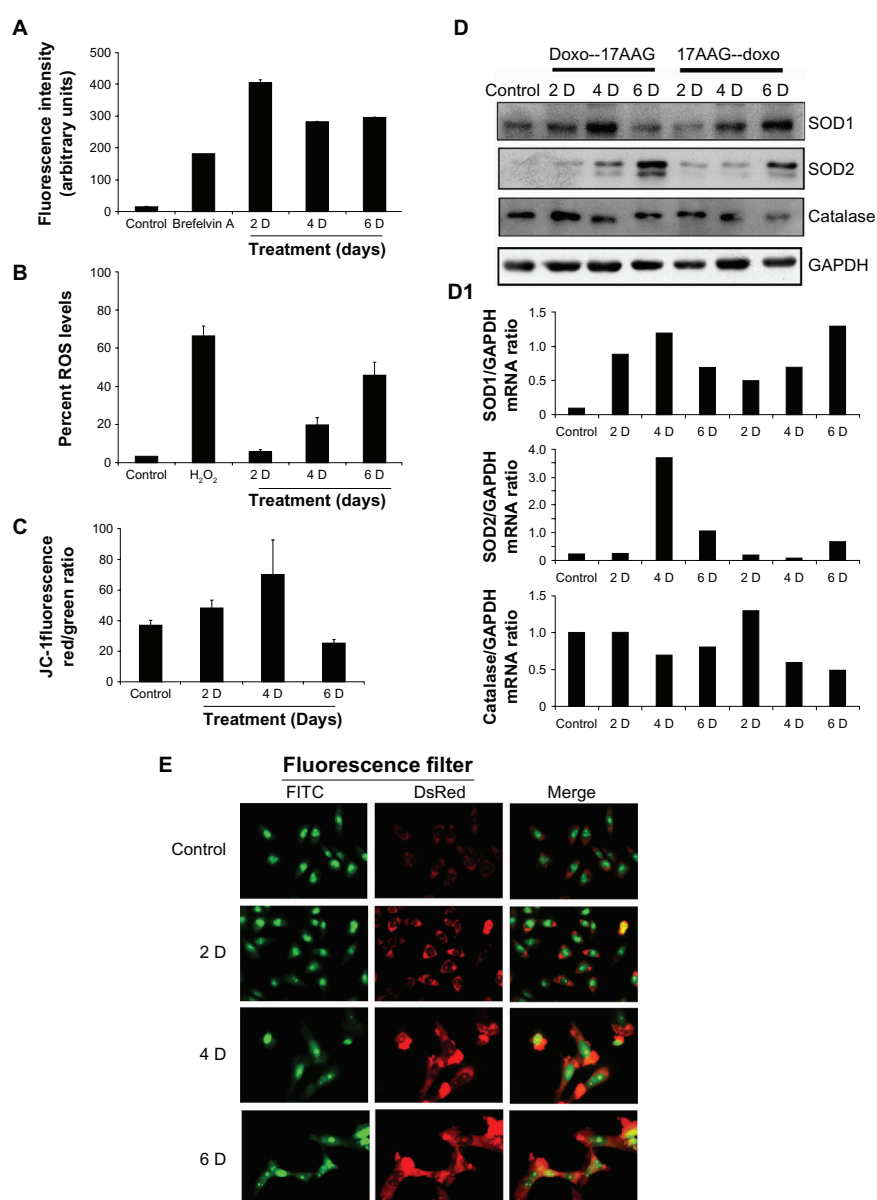


Figure 4. Effects of 17AAG pre-treatment on cellular redox status. **(A)** $[[Ca^{2+}]_i]$ was measured by staining cells with Fluo3-AM and analyzed by FACS. Brefeldin A was used as positive control to induce Ca^{2+} release into the intracellular milieu. **(B)** $[(ROS)]_i$ was measured by incubating cells with CM- H_2DCFDA and analyzing the green fluorescence by FACS. Hydrogen peroxide (H_2O_2) was used as a positive control to induce $[(ROS)]_i$ levels. **(C)** A change in mitochondrial membrane potential ($\Delta\Psi_m$) was measured by staining cells with JC-1 fluorophore and analyzing in FACS. An increase in red to green fluorescence ratio was plotted in the bar diagram. **(D)** RT-PCR analyses with gene specific primers for *SOD1*, *SOD2* and *catalase*. The GAPDH amplification was used as input. **(D1)** The densitometric values of GAPDH vs. individual gene expression ratios was represented in the bar diagram. **(E)** Staining of autophagic vacuoles. Cells were incubated with acridine orange to stain acidic lysosomes characteristic of autophagy. Green indicates nuclear staining and red indicates acidic lysosomal staining. Scale bar represents 25 μm at 100 \times magnification in a laser scanning confocal imaging microscope, Leica TCS SP5.

versus GAPDH ratio (Fig. 4D1). In agreement with moderate increases in oxidative stress that correlated to sensitizing effects of cellular senescence²⁷ but not to apoptosis, we also observed a moderate increase in $[(ROS)]_i$. Since senescent cells are usually resistant to apoptosis or necrosis, removal of damaged cells could occur by autophagy (type II programmed cell death). Accordingly, senescent cells showed enhanced

acridine orange staining, a characteristic feature of macroautophagy¹⁴ (Fig. 4E).

17AAG pre-treatment induced senescence is irreversible

Pharmacological modulator curcumin was shown to promote proliferation in neuroblastoma,⁶ therefore, we examined the effect of curcumin on reversal

of senescence. Although curcumin (15 μ M, 24 h) increased the number of SA- β -gal positive cells in a day-3 treatment ($>133\%$, $P < 0.05$), which is significantly decreased by day-5 treatment ($<37\%$, $P < 0.05$). These data (Fig. 5A) suggests that senescent cells did not respond to proliferation stimulus. We further examined the proliferation stimulus using epidermal growth factor (EGF, 50 nM) on senescent cells. EGF treatment increased subG1 cells by decreasing both G1/S and

G2/M populations suggesting enhanced cytotoxicity (Fig. 5B).

The mTOR, a serine/threonine kinase activation favors senescence in tumor cells.²⁸ To investigate the involvement of mTOR signaling in senescence, cells were treated with mTOR inhibitor, rapamycin for 48 h and compared with rapamycin (200 nM) combined 17AAG pre-treatments at day 2, 4, and 6 using FACS. While rapamycin had no effect on control cells, its treatment to senescence directed cells resulted in

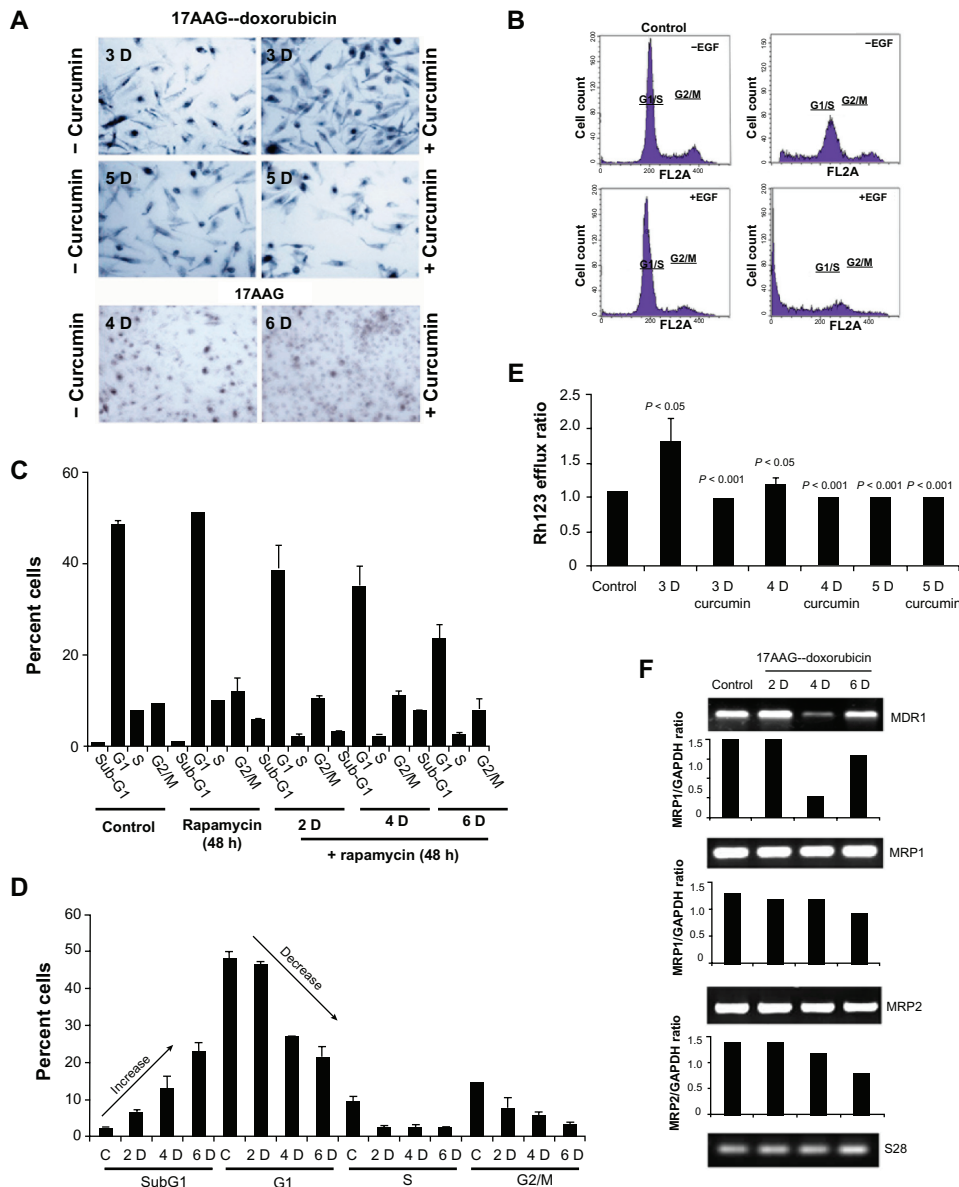


Figure 5. Studies on 17AAG pre-treatment accelerated senescence reversal. (A) Cells after treatment with respective senescence inducers were incubated with curcumin for 24 h and examined for SA- β -gal positive cells. (B) Cells after day 6 of the treatment were stimulated with EGF for 24 h and analyzed by FACS. (C) Senescent cells were incubated with rapamycin for 48 h and analyzed by FACS. (D) Cells were incubated with wortmanin for 18 h and analyzed by FACS. (E) Rh123 efflux was calculated in presence and absence of 2 h pre-incubation with curcumin. Cyclosporin A was used to study the maximum retention of Rh123. (F) RT-PCR analyses of *MDR1*, *MRP1* and *MRP2* of cells after 17AAG pre-treatment. S28 RNA vs. individual gene expression ratios were represented in the bar diagram.



a decrease to G1 and increase to subG1 population suggesting that compromised mTOR functions compromises cell survival (Fig. 5C, $P < 0.001$). In addition to mTOR, PI3 serine/threonine kinase (PI3K) has been implicated in senescence.²⁸ Therefore, we looked for the effect of PI3K inhibitor, wortmanin (200 nM) on senescent cells by using FACS. Wortmanin treatment also resulted in increased cell death suggesting its role in senescence cell survival (Fig. 5D, $P < 0.001$).

Enhanced multidrug resistance (MDR) is one of the characteristic features of senescent cells.²⁹ To understand whether senescent cells show any enhanced drug resistance, we examined for Rh123 efflux of cells from day 3, 4 and 5 of the treatment. Since curcumin interferes with MDR functions, curcumin was used (2 h pre-treatment prior to Rh123 efflux assay) to inhibit MDR functions. Compared to control efflux ratio, which was due to constitutive MDR activation in IMR-32 (9), 3-day treatments showed increased efflux ratio by 0.5 folds, suggesting enhanced functions of MDR on the onset of senescence. Further, curcumin was effective in decreasing MDR functions as observed by Rh123 efflux (Fig. 5E). Concurrently, decreased *MDR1* expression by 4-days and its re-expression by 6-days were observed. The chronic expressions of multidrug related proteins, *MRP1* and *MRP2* were however, not affected by senescence activation (Fig. 5F). The representative Image J analysis of gene expression versus GAPDH was shown in bar diagram.

Senescent cells show compromised colony forming ability and neo-vascularization

It was reported that only a subset of cancer cells respond to drug induced cellular senescence and remaining cells retain metastatic potential and lead to recurrence.^{30,31} To exclude the possibility of tumor relapse in our senescence model, first we examined anchorage-independent cell growth using soft agar colony formation assay. Cells from post 17AAG pre-treatments at day 2, 4 and 6 were placed on agarose coated surface and the proliferation potential of cells was monitored for colony forming ability. Cells collected on the onset of senescence showed $\pm 65\%$ decrease in colony size (Fig. 6A and 6A1). Next,

we examined for neo-vascularization after growing cells on matrigel coated surface. A 6-day growth of control cells on matrigel resulted in organized large colonies. However, cells from the onset of senescence showed a significant decrease in the organized colony structures (Fig. 6B). These findings are consistent with SA- β -gal data that a majority of cells enter senescence state, which acts as an anti-proliferative and anti-metastatic mechanism. Cells that fail to enter senescence state were found to be eliminated by cytotoxicity (compare Fig. 2 with Suppl. Fig. 2B).

Compromising Hsp90 expression compromises survival potential of senescent cells

We show that interference with high affinity conformation of Hsp90 with 17AAG³² accelerates doxorubicin induced senescence. In these experiments 17AAG treatment *per se* will not affect Hsp90 expression or its synthesis, but interferes with its high affinity conformation. Therefore, to study whether compromised Hsp90 expression will have any effect on senescence activation, IMR-32 cells on the onset of senescence were transiently transfected with siRNA to knockdown Hsp90 (2 μ g/ 0.4×10^6 cells). After 24 h siRNA treatment, knockdown of Hsp90 expression was confirmed by examining the *hsp90* mRNA levels (Suppl. Fig. 3). Subsequently, cells were tested for SA- β -gal staining and cytotoxicity. A significant decrease in SA- β -gal positive cells in day-2, -4 and -6 (Fig. 6C and D, $P < 0.05$) with a concomitant increase in cytotoxicity (Fig. 6E) implied that Hsp90 expression is indispensable for cell survival. Chronic expression of Hsp90 is required for cell survival, but not the high affinity conformation, where the latter is involved in oncogenic signal transduction and enhanced cell proliferation.^{32,33}

CM-SASPs from senescent cells induce senescence

Enforced senescence in tumor cells has also been proposed to be deleterious, because it activates age-associated pathologies.³⁴ The genotoxic stress enhances senescence associated secretory phenotype (SASP), which however, is linked to the loss of p53 function or enhanced oncogene activation.³⁵ Since, IMR-32

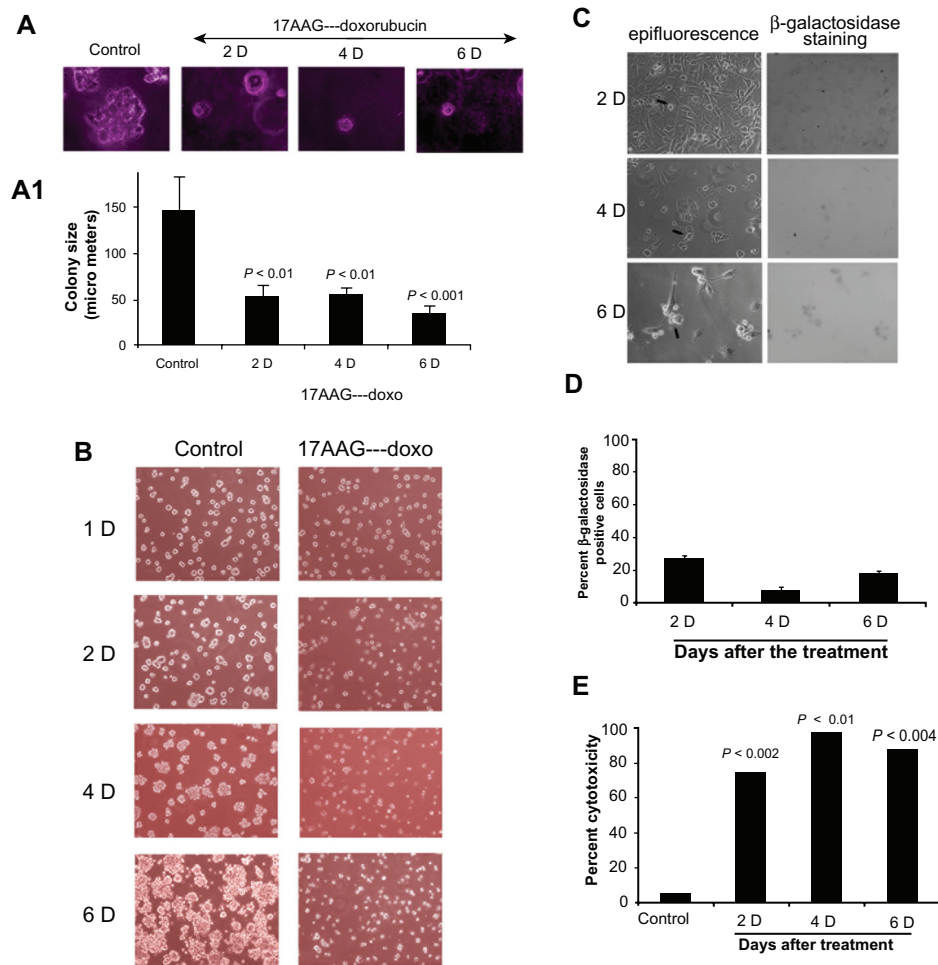


Figure 6. Anti-proliferative/anti-neo-vascularization effects of 17AAG pre-treatment accelerated senescence cells. **(A)** Anchorage-independent cell growth analysis of 17AAG pre-treated cells for 14-days on agar coated plates. **(A1)** Increase in colony size represents growth stimulus and proliferation potential, note that senescence cells showing decreased proliferation potential. **(B)** Anchorage-dependent growth on matrigel coated glass surface. Note a decrease in organized colonies on the onset of senescence. **(C)** Effect of siRNA knockdown of Hsp90 on SA- β -gal positive cells on 17AAG pre-treatments. **(D)** Counting of SA- β -gal positive cells after 17AAG pre-treatments. **(E)** The cytotoxicity analysis of siRNA knockdown of Hsp90. The increase in cytotoxicity was assessed by the accumulation of percent subG1 cells.

exhibit functional p53 and chronic oncogene activation, we examined CM containing SASPs from senescent cells on pro-senescence activity. Between the two cell types used in our study, jurkat cells mimic T-cell leukemia and secrete cytokines, whereas, SRA01 are virus free immortalized cells containing progenitors of myoepithelial lacking tumorigenic activity. The CM treated tumor cells showed senescence morphology by 4-day treatment as observed by SA- β -gal staining. Interestingly, between jurkat and SRA01, the SRA01 showed 50% less SA- β -gal positive cells, however, were associated with enhanced cytotoxicity. These experiments suggested that the paracrine activities of SASPs in our model lack tumor promoting factors but retained senescence activating factors (Fig. 7A).

Discussion

Neuroblastoma has been considered as a malignant manifestation of aberrant sympathetic nervous system development. Irreconcilable differences in therapeutic strategies due to high tumor heterogeneity limit existing approaches, thus, insist on developing novel strategies, which can exploit the oncogenic signatures of tumor cells.³⁶ Earlier, we showed that pharmacological targeting of Hsp90 functions deprives proliferation promoting signal transduction in IMR-32 neuroblastoma, however, the apparent recurrence on post-treatment suggested limitations to this approach.^{6,37} In this study, we demonstrate how compromising the chaperoning functions of Hsp90 (17AAG pre-treatment) sensitizes neuroblastoma to doxorubicin induced

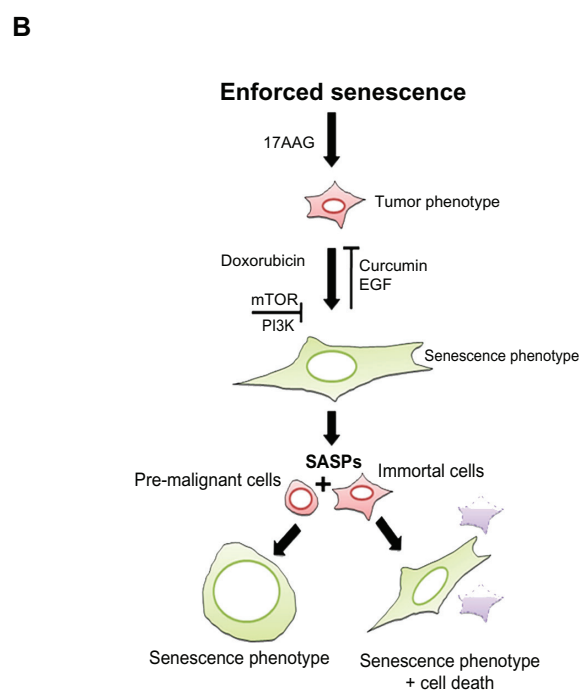
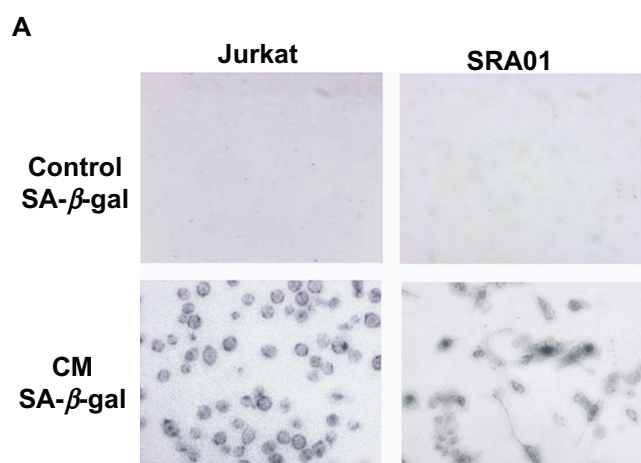


Figure 7. (A) conditioned medium induced senescence activity in jurkat and SRA01 cells. The conditioned medium from 17AAG pre-treatment accelerated senescence cells was examined for pro-senescence activity in pre-malignant (jurkat) and immortal cells (SRA01) for 6-days and cells were stained for SA- β -gal activity. Note decreased number of SA- β -gal positive cells in SRA01 cells compared to jurkat cells. (B) Proposed senescence activation model.

cellular senescence, and present conformation specific Hsp90 as a barrier to enforced senescence of tumor cells.

Although Hsp90 is an exciting drug target due to its cancer specificity it is likely to induce drug resistance over time.³⁸ Some Hsp90 inhibitors can induce oxidative stress leading to non-specific actions in tumor cells and may also affect bystander cells.³⁹

However, in the present study, microgram concentrations of 17AAG for prolonged incubation periods is required to obtain 50% cells death, which may develop drug resistance in cancer cells in due course of time. Similar findings with doxorubicin suggested ability of cells to resist chemotherapeutic intervention. Although combination drug treatment has improved the cytotoxic effects of drugs in earlier time periods, prolonged periods of incubation suggested either delayed drug response or acquired drug resistance (Supplemental Fig. 1B). Doxorubicin pre-treatment followed by 17AAG did not improve efficacy of cytotoxic treatment strategy, but 17AAG-pretreatment has significantly decreased cytotoxicity (Supplemental Fig. 2B). To our surprise, SA- β -gal staining indicative of senescence was observed in 17AAG pre-treatments suggesting bypassing chemotherapeutics induced cytotoxicity results in cellular senescence. The increase in SA- β -gal positive cells was almost doubled in 17AAG pre-sensitization compared to doxorubicin treatment alone (compare Fig. 1A1 with Fig. 2A1).

In recent years, enforcing premature senescence in tumor cells with chemotherapeutic mediation has been proposed as an alternate strategy to combat cancers.^{40,41} Prolonged cytostasis either through p53-p21^{CIP/WAF-1} or pRb-p16^{INK4a} meditation was thought to be the focal point in such models.⁴² Despite the fact that individual drug treatments do not show significant increase in p21^{CIP/WAF-1} expression, the combination treatment showed increased p21^{CIP/WAF-1} expression correlating with p53 (compare Fig. 1B and C with Fig. 2D and E) that however, did not result in increased senescence positive cells (compare Fig. 1A1 with Fig. 2A1). The increased p21^{CIP/WAF-1} expression only in 17AAG pre-treatment but not in doxorubicin pre-treatment resulted in increased senescence positive cells (Fig. 2). Although, replicative senescence is linked to p16^{INK4a}, in our study, incessant p16^{INK4a} over expression was found to have no influence on induced senescence signaling in individual and combination drug treatments (Fig. 1), but its decrease in 17AAG pre-treatment resulted in significant increase in senescence positive cells (Fig. 2). We speculate that p16^{INK4a} may be antagonizing senescence signaling induced by chemotherapeutic interventions. In accordance with this, p16^{INK4a} constitutive expression²² has been



implicated in bypassing cellular senescence.⁴³ We are in the process of examining the role of p16^{INK4a} in tumor metastasis and bypassing induced senescence. Excluding p16^{INK4a} in 17AAG pre-treatment induced senescence, the senescence observed in our model is pragmatic to p53-p21^{CIP/WAF-1} mediation.

Interestingly, the stress proteins (Hsp27, Hsp70 and Hsp90) that showed fluctuations in individual and combination drug treatments (Fig. 1) were not significantly affected by the followed drug treatments (Fig. 2) implicating functional compromise but not expression levels play role in altering the cell fate. Consistent with this stabilized p53 and p21^{CIP/WAF-1} levels appeared to play significant role in cellular decision correlating with differentially regulated cdks. In accordance with this we did not find complete loss of proliferation (PI3K-AKT) or survival (Ras-Raf-ERK) signal transduction but their apparent alteration (Fig. 1 and Fig. 2). The continued kinase activities may therefore relate to cellular crisis induced by the combination drug treatments. The data obtained from Figures 1 and 2 however failed to conform to any classical signal transduction pathway leading to senescence, it confirmed that senescence occurred through p53-p21^{CIP/WAF-1} mediation. With this lead we went ahead for further characterization of senescence.

Enhanced SAHF is involved in maintaining the senescence phenotype. Although SA- β -gal staining can be used to detect both cellular stress response as well as senescence response, increased SA- β -gal staining with increased nucleus to cytoplasm ratio indicated the onset of senescence (Supplemental Figs. 1A and 2A), which further correlated with a time dependent increase in SAHF staining (Fig. 3D). Our results may differ with the findings of Restall and Lorimer,⁴⁴ who reported that Hsp90 inhibition alone can induce premature senescence in small cell lung carcinoma (SCLC). The SAHF increase in their study has been correlated to senescence associated with DDR response to DNA damage. Studies from different groups indicate that Hsp90 inhibition *per se* will not induce DNA damage but compromises DDR.^{45,46} We bring forth evidence from the present study that compromising the chaperoning functions of Hsp90 with 17AAG enhances the doxorubicin induced DDR in neuroblastoma. Another marker of senescence, H3K4me3 suggests increased patterns of histone acetylation and competence of transcriptional

activation⁴⁷ thus negates SAHFs. However, in the present model, H3K4me3 cytoplasmic accumulation has invalidated its role in active chromatin transcription. Nevertheless, F-actin re-organization and increased cell granularity together with non-functional telomerases has appraised telomerase-independent senescence activation (Fig. 3).

Physiological factors such as ROS and Ca²⁺ were also implicated in senescence signaling. In fact aging phenotypes were thought to be established through oxidative signaling. Since Hsp90 inhibitors alone can elevate ROS,³⁹ in the present study, the ROS mediated senescence activation^{48,49} cannot be exempted. To our surprise, we observed only a small but gradual increase in ROS levels, which were addressed by the activated mitochondrial antioxidant defense. These findings sets aside the role of ROS in senescence activation.^{27,50,51} Although Hsp90 inhibition induces the release of intracellular Ca²⁺,⁵² in a rat tumor model, this release was then correlated to decreased functions of Hsps.⁵³ Unlike the rat model where Hsp gene transcription was found to be compromised, IMR-32 cells retained some Hsps suggesting survival potential of cells upon elevated Ca²⁺ levels. Reinforcing this, the increased calcium levels correlated with the activation of senescence response but not apoptosis (Fig. 4). In previous sections we discussed how senescent cells are resistant to cell death mechanisms such as apoptosis under conditions of depleted oxygen stress⁵⁴ and now in agreement with this, in the present study, we observed activation of autophagy, which was considered to be pro-survival response mechanism.

Senescence mediated by p53-p21^{CIP/WAF-1} has been reported to be reversible therefore may limit the application of our strategy. Failing to induce senescence reversal with mTOR inhibitor, EGF or curcumin that were known to decelerates senescence,^{55,56} appraise that enforced proliferation stimulus is inoperative once senescence signal is being activated. In accordance with earlier understanding that synergistic activation of PI3K and mTOR provide survival fitness to cancer cells,⁵⁷ and their chronic activation lead to senescence,⁵⁸ we demonstrated that drug treatments promote senescence through chronic signal activation (Fig. 5). Therefore the irreversible potential of tumor cells may relate to enhanced senescence-associated multi drug resistance.⁵⁹ Doxorubicin being



the substrate of multi drug resistance gene product, MDR1,⁶⁰ it was presumed that Hsp90 inhibition promotes its bioavailability to exhibit enhanced senescence activity. With the prelude that Hsps promote multidrug resistance in tumor cells, we interpret that functional Hsp90 inhibition in MDR1 positive⁹ IMR-32 cells could possibly have primarily compromised the drug efflux, thus could have increased doxorubicin cellular accumulation to promote senescence associated effects.

The augmentation of doxorubicin induced senescence by Hsp90 inhibitors in neuroblastoma suggests an alternate strategy to combat cancers. Evaluation whether enforced cellular senescence act as a tumor suppression mechanism by anchorage independent (growth on agarose) and anchorage dependent (growth on matrigel) growth assays revealed anti-proliferative and anti-angiogenic competence. However, in contrast to compromising of Hsp90 chaperoning function using pharmacological drugs, knockdown of Hsp90 using siRNA has significantly compromised the survival potential of senescent population (Fig. 6) suggesting Hsp90 expression is indispensable for cell survival whether cells are from normal, tumor or senescent groups.

Paradoxically chemotherapeutic drugs must exert two important tumor suppressor mechanisms namely, senescence or apoptosis. Hsps antagonize apoptotic signaling^{1,53} but facilitates senescence.⁶¹ The conformational maturation and functional stabilization of oncogenes was aided by conformation specific Hsp90 (high affinity conformation) present in tumor cells, which is in addition to the presence of normal Hsp90 (low affinity conformation).³² In the present study, pre-sensitization of tumor cells with conformation specific anti-Hsp90 inhibitor, 17AAG to doxorubicin treatment suggested that by compromising high affinity conformation of Hsp90 it may be possible to sensitize Hsp90 inhibition resistant tumor cells to chemotherapeutic intervention. Our results demonstrate that Hsp90 in its high affinity conformation undeniably acts as an impediment to senescence signaling due to its involvement in tumor progression. Our findings are in agreement with earlier hypothesis that decreased chaperoning functions of Hsps promote senescence signaling.^{62,63}

Findings from Campici's group⁶⁴ though projected enforced cellular senescence as a tumor suppressor mechanism, later findings from the same group showed that factors secreted to the culture medium (condition medium-CM) by senescent cells (SASPs) can promote transformation in pre-malignant cells.^{34,65} These findings invalidated the strategy of enforced cellular senescence for antitumor treatment.⁶⁶ Nevertheless, we project that CM from 17AAG pre-treatment induced senescent cells lack proliferation stimulus as envisioned by other groups but interestingly accelerated senescence-like phenotype in target cells (Fig. 7A). The disparity in SASPs from others to our study was found to be only the use of Hsp90 inhibition to accelerate senescence. Our findings, therefore, may have clinical benefits for cutting-edge treatments using anti-Hsp90 drugs. For thorough understanding of the molecular cross-talk in neuroblastoma, at this point in time we are characterizing SASPs and also investigating the functional silencing of p16^{INK4a} and its contribution in bypassing senescence in IMR-32 cells.

In summary, both cancer and senescence cells express high amounts of Hsps, however, differ in their chaperoning activities. While enhanced chaperoning functions of Hsp90 with increased ATP binding affinity promote tumor progression allowing mutated gene products to function normally, the basal functions help to maintain protein homeostasis. Taking leads from these findings, we manipulated the chaperone functions of Hsp90 and studied genotoxic drug-induced cellular senescence in IMR-32 neuroblastoma. Among different individual and combination drug treatments, pre-sensitization of neuroblastoma with 17AAG accelerated doxorubicin induced DDR and signaled cells to stress induced cellular senescence. Despite its known functions in replicative senescence^{67,68} we demonstrate how DDR signaling promote stress-induced senescence. Several cellular factors, signaling molecules and second messengers that have contributed to enforced senescence in IMR-32 neuroblastoma were discussed. Essentially Hsp90 as a barrier for enforced senescence in tumor cells was emphasized (Fig. 7B). Our findings add contemporary information, attractive strategy and effective therapeutic option wherein exploitation of conformation specific Hsp90 in sensitizing metastatic tumor cells leads to enforced cellular senescence.



Author Contributions

US, KRP, JUK and VS performed the experiments and acquired the data. ASS conceived the hypothesis, designed the experiments, analyzed the data and wrote the manuscript.

Abbreviations

Hsp, heat shock protein; Hsp90, 90 kDa heat shock protein; 17AAG, 17-allylamino-17-demethoxygeldanamycin; SA- β -gal, senescence-associated β -galactosidase; H3K4me3, Trimethylation of histone H3 at lysine 4; DDR, DNA damage response; γ H₂AX, phosphorylated histone H2A; [(ROS)i], intracellular reactive oxygen species; [(Ca²⁺)i], intracellular calcium; $\Delta\Psi$ m, change in mitochondrial membrane potential; CM, conditioned medium; SASP, senescence-associated secretory phenotype; SAHF, senescence associated heterochromatin foci; Rh123, Rhodamine 123; FACS, fluorescence activated cell sorting; MDR1, multidrug resistance gene; MRP, multidrug related protein; p21^{CIP/WAF-1}, p21 cdk interacting protein 1/wild type p53 activated fragment 1; p16^{INK4a}, p16 inhibitors of CDK4; SOD, super oxide dismutase; siRNA, small interfering RNA.

Funding

This work was supported by grants to ASS from Department of Science and Technology, Government of India.

Competing Interests

Author(s) disclose no potential conflicts of interest.

Disclosures and Ethics

As a requirement of publication author(s) have provided to the publisher signed confirmation of compliance with legal and ethical obligations including but not limited to the following: authorship and contribution, conflicts of interest, privacy and confidentiality and (where applicable) protection of human and animal research subjects. The authors have read and confirmed their agreement with the ICMJE authorship and conflict of interest criteria. The authors have also confirmed that this article is unique and not under consideration or published in any other publication, and that they have permission from rights holders to reproduce any copyrighted material. Any disclosures are made in this section. The external blind peer reviewers report no conflicts of interest.

References

1. Sreedhar AS, Csermely P. Heat shock proteins in the regulation of apoptosis: new strategies in tumor therapy: a comprehensive review. *Pharmacol Ther.* 2004;101:227–54.
2. Whitesell L, Lindquist S. Hsp90 and the chaperoning of cancer. *Nat Rev Cancer.* 2005;5:761–72.
3. Cid C, Regidor I, Poveda PD, Alcazar A. Expression of heat shock protein 90 at the cell surface in neuroblastoma cells. *Cell Stress and Chaperones.* 2009;14:321–7.
4. Sumizawa T, Igishu H. Release of heat shock proteins from neuroblastoma cells exposed to acrylamide. *J Toxicol Sci.* 2008;33:117–22.
5. Kim S, Kang J, Hu W, Evans BM, Chung DH. geldanamycin decreases Raf-1 and Akt levels and induces apoptosis in neuroblastomas. *Int J Cancer.* 2003;103:352–9.
6. Taiyab A, Srinivas UK, Sreedhar AS. 17-(Allylamino)-17-demethoxygeldanamycin combination with diferuloylmethane selectively targets mitogen kinase pathway in a human neuroblastoma cell line. *J Cancer Ther.* 2010;1:197–204.
7. Pratt WB, Toft DO. Regulation of signaling protein function and trafficking by the hsp90/hsp70-based chaperone machinery. *Exp Biol Med (Maywood).* 2003;228:111–33.
8. Sreedhar AS, Soti C, Csermely P. Inhibition of Hsp90: a new strategy for inhibiting protein kinases. *Biochim Biophys Acta.* 2004;1697:233–42.
9. Xue C, Haber M, Flemming C, et al. p53 determines multidrug resistance of childhood neuroblastoma. *Cancer Res.* 2007;67:10351–60.
10. Diccianni MB, Omura-Minamisawa M, Batova A, Le T, Bridgeman L, Yu AL. Frequent deregulation of p16 and p16/G1 cell cycle-regulatory pathway in neuroblastoma. *Int J Cancer.* 1999;80:145–54.
11. Wendel HG, De Stanchina E, Fridman JS, et al. Survival signalling by Akt and eIF4E in oncogenesis and cancer therapy. *Nature.* 2004;28:332–7.
12. Fulda S. Apoptosis and neuroblastoma therapy. *Curr Pharma Des.* 2009;9:729–37.
13. Dimri GP, Lee X, Basile G, et al. Biomarker that identifies senescent human cells in culture and in aging skin in vivo. *Proc Natl Acad Sci U S A.* 1995;92:9363–7.
14. Kurz DJ, Decary S, Hong Y, Erusalimsky JD. Senescence-associated (beta)-galactosidase reflects an increase in lysosomal mass during replicative ageing of human endothelial cells. *J Cell Sci.* 2000;113:3613–22.
15. Kwak IH, Kim HS, Choi OR, Ryu MS, Lim IK. Nuclear accumulation of globular actin as a cellular senescence marker. *Cancer Res.* 2004;64:572–80.
16. Lee S, Jeong SY, Lim WC, et al. Mitochondrial fission and fusion mediators, hFis1 and OPA1, modulate cellular senescence. *J Biol Chem.* 2007;282:22977–83.
17. Hwang ES, Yoon G, Kang HT. A comparative analysis of the cell biology of senescence and aging. *Cell Mol Life Sci.* 2009;66:2503–24.
18. Shammas MA, Koley H, Batchu RB, et al. Telomerase inhibition by siRNA causes senescence and apoptosis in Barrett's adenocarcinoma cells: mechanism and therapeutic potential. *Mol Cancer.* 2005;4:24.
19. Ke XS, Qu Y, Rostad K, et al. Genome-wide profiling of histone h3 lysine 4 and lysine 27 trimethylation reveals an epigenetic signature in prostate carcinogenesis. *PLoS ONE.* 2009;4:e4687.
20. Pospelova TV, Demidenko ZN, Bukreeva EI, Pospelov VA, Gudkov AV, Blagosklonny MV. Pseudo-DNA damage in response in senescent cells. *Cell Cycle.* 2009;8:4112–8.
21. Beausejour CM, Krtolica A, Galimi F, et al. Reversal of human cellular senescence: roles of the p53 and p16 pathways. *EMBO J.* 2003;22:4212–22.
22. Omura-Minamisawa M, Diccianni MB, Chang RC, et al. p16/p14(ARF) cell cycle regulatory pathways in primary neuroblastoma: p16 expression is associated with advanced stage disease. *Clin Cancer Res.* 2001;7:3481–90.
23. Huang MS, Adebajo OA, Awumey E, et al. IP(3), IP(3) receptor, and cellular senescence. *Am J Physiol Renal Physiol.* 2000;278:F576–84.
24. Beckman KB, Ames BN. The free radical theory of aging matures. *Physiol Rev.* 1998;8:547–81.



25. Vayssier-Taussat M, Kreps SE, Adrie C, Ava JD, Christiani D, Polla BS. Mitochondrial Membrane Potential: A Novel Biomarker of Oxidative environmental Stress. *Envir Health Perspect*. 2002;110:301–5.
26. Sohal RS, Weindruch R. Oxidative stress, caloric restriction, and aging. *Science*. 1996;273:59–63.
27. Passos JF, von Zglinicki T, Saretzki G. Mitochondrial dysfunction and cell senescence: cause or consequence? *Rejuvenation Res*. 2006;9:64–8.
28. Collado M, Medema Rene H, Garcia-Cao I, et al. Inhibition of the phosphoinositide 3-kinase pathway induces a senescence-like arrest mediated by p27^{Kip1}. *J Biol Chem*. 2000;275:21960–8.
29. Achuthan S, Santhoshkumar TR, Prabhakar J, Nair SA, Pillai MR. Drug-induced senescence generates chemoresistant stemlike cells with low reactive oxygen species. *J Biol Chem*. 2011;286:37813–29.
30. Ewald JA, Desotelle JA, Wilding G, Jarrard DF. Therapy-induced senescence in cancer. *J Natl Cancer Inst*. 2010;102:1536–46.
31. Michishita E, Nakabayashi K, Ogino H, Suzuki T, Fujii M, Ayusawa D. DNA topoisomerase inhibitors induce reversible senescence in normal human fibroblasts. *Biochem Biophys Res Comm*. 1998;253:667–71.
32. Kamal A, Thao L, Sensintaffar J, et al. A high-affinity conformation of Hsp90 confers tumour selectivity on Hsp90 inhibitors. *Nature*. 2003;425:407–10.
33. Csermely P, Schnaider T, Soti C, Pohaszka Z, Nardai G. The 90-kDa molecular chaperone family: structure, function, and clinical applications. A comprehensive review. *Pharmacol Ther*. 1998;79:129–68.
34. Coppe JP, Desprez PY, Krtolica A, Campisi J. The senescence-associated secretory phenotype: the dark side of tumor suppression. *Annu Rev Pathol* 2010;5:99–118.
35. Coppe JP, Patil CK, Rodier F, et al. Senescence-associated secretory phenotypes reveal cell-nonautonomous functions of oncogenic RAS and the p53 tumor suppressor. *PLoS Biol*. 2008;6:2853–68.
36. Maris JM. Recent advances in neuroblastoma. *N Engl J Med*. 2010;362:2202–11.
37. Jyothidi D, Vanathi P, Mangala Gowri O, Rama Subba Rao V, Madhusudhan Rao J, Sreedhar AS. Diferuloylmethane augments the cytotoxic effects of piplartine isolated from Piper chaba. *Toxicol In Vitro*. 2009;23:1085–91.
38. Kamal A, Burrows FJ. Hsp90 inhibitors as selective anticancer drugs. *Discov Med*. 2004;4:277–80.
39. Sreedhar AS, Mihaly K, Pato B, et al. Hsp90 inhibition accelerates cell lysis: anti-Hsp90 ribozyme reveals a complex mechanism of Hsp90 inhibitors involving both superoxides- and Hsp90-dependent events. *J Biol Chem*. 2003;278:35231–40.
40. Di Micco R, Sulli G, Dobrev M, et al. Interplay between oncogene-induced DNA damage response and heterochromatin in senescence and cancer. *Nat Cell Biol*. 2011;13:292–302.
41. Spallarossa P, Altieri P, Aloï C, et al. Doxorubicin induces senescence or apoptosis in rat neonatal cardiomyocytes by regulating the expression levels of the telomere binding factors 1 and 2. *Am J Physiol Heart Circ Physiol*. 2009;297:H2169–81.
42. Aprelikova O, Xiong Y, Liu ET. Both p16 and p21 families of cyclin-dependent kinase (CDK) inhibitors block the phosphorylation of cyclin-dependent kinases by the CDK-activating kinase. *J Biol Chem*. 1995;270:18195–7.
43. Romagosa C, Simonetti S, Lopez-Vicente L, et al. p16(Ink4a) overexpression in cancer: a tumor suppressor gene associated with senescence and high-grade tumors. *Oncogene*. 2011;30:2087–97.
44. Restall IJ, Lorimer IA. Induction of premature senescence by hsp90 inhibition in small cell lung cancer. *PLoS One*. 2010;5:e11072.
45. Dote H, Burgan WE, Camphausen K, Tofilon PJ. Inhibition of Hsp90 compromises the DNA damage response to radiation. *Cancer Res*. 2006;66:9211–20.
46. Ha K, Fiskus W, Rao R, et al. Hsp90 inhibitor-mediated disruption of chaperone association of ATR with hsp90 sensitizes cancer cells to DNA damage. *Mol Cancer Ther*. 2011;10:1194–206.
47. Barski A, Cuddapah S, Cui K, et al. High-resolution profiling of histone methylations in the human genome. *Cell*. 2007;129:823–37.
48. Noor R, Mittal, S, Iqbal J. Superoxide dismutase—applications and relevance to human diseases. *Med Sci Monit*. 2002;8:RA210–05.
49. Dery E, Gosselin K, Vercamer C, et al. MnSOD upregulation induces autophagic programmed cell death in senescent keratinocytes. *PLoS One*. 2010;5:e12712.
50. Marchi S, Giorgi C, Suski JM, et al. Mitochondria-ros crosstalk in the control of cell death and aging. *J Signal Transduct*. 2012:329635.
51. Jahangir A, Ozcan C, Holmuhamedov EL, Terzic A. Increased calcium vulnerability of senescent cardiac mitochondria: protective role for a mitochondrial potassium channel opener. *Mech. Ageing Dev*. 2001;122:1073–86.
52. Taiyab A, Sreedhar AS, Rao CM. Hsp90 inhibitors, GA and 17AAG, lead to ER stress-induced apoptosis in rat histiocytoma. *Biochem Pharmacol*. 2009;78:142–52.
53. Sreedhar AS, Pardhasaradhi BV, Begum Z, Khar A, Srinivas UK. Lack of heat shock response triggers programmed cell death in a rat histiocytic cell line. *FEBS Lett*. 1999;456:339–42.
54. Afanas'ev I. Reactive oxygen species signaling in cancer: comparison with aging. *Ageing Dis*. 2011;2:219–30.
55. Demidenko ZN, Zubova SG, Bukreeva EI, Pospelov VA, Pospelova TV, Blagosklonny MV. Rapamycin decelerates cellular senescence. *Cell Cycle*. 2009;8:1888–95.
56. Park WY, Cho KA, Park JS, Kim DI, Park SC. Attenuation of EGF signaling in senescent cells by caveolin. *Ann N Y Acad Sci*. 2001;928:79–84.
57. Ayril-Kaloustian S, Gu J, Lucas J, et al. Hybrid inhibitors of phosphatidylinositol 3-kinase (PI3K) and the mammalian target of rapamycin (mTOR): design, synthesis, and superior antitumor activity of novel wortmannin-rapamycin conjugates. *J Med Chem*. 2010;53:452–9.
58. Astle MV, Hannan KM, Ng PY, et al. AKT induces senescence in human cells via mTORC1 and p53 in the absence of DNA damage: implications for targeting mTOR during malignancy. *Oncogene*. 2012;31:1949–62.
59. Yan Q, Wajapeyee N. Exploiting cellular senescence to treat cancer and circumvent drug resistance. *Cancer Biol Ther*. 2010;9:166–75.
60. Shen F, Chu S, Bence AK, et al. Quantitation of doxorubicin uptake, efflux, and modulation of multidrug resistance (MDR) in MDR human cancer cells. *J Pharmacol Exp Ther*. 2008;324:95–102.
61. Soti C, Sreedhar AS, Csermely P. Apoptosis, necrosis and cellular senescence: chaperone occupancy as a potential switch. *Ageing Cell*. 2003;2:39–45.
62. Soti C, Csermely P. Molecular chaperones and the aging process. *Biogerontology*. 2000;1:225–33.
63. Csermely P. Chaperone overload is a possible contributor to 'civilization diseases'. *Trends Genet*. 2001;17:701–4.
64. Campisi J. Cancer, aging and cellular senescence. *In Vivo*. 2000;14:183–8.
65. Krtolica A, Parriello S, Lockett S, Desprez PY, Campisi J. Senescent fibroblasts promote epithelial cell growth and tumorigenesis: a link between cancer and aging. *Proc Nat Acad Sci U S A*. 2001;98:12072–7.
66. Young AR, Narita M. SASP reflects senescence. *EMBO Rep*. 2009;10:228–30.
67. Gire V, Roux P, Wynford-Thomas D, Brondello JM, Dulic V. DNA damage checkpoint kinase Chk2 triggers replicative senescence. *EMBO J*. 2004;23:2554–63.
68. Mallette FA, Gaumont-Leclerc MF, Ferbeyre G. The DNA damage signaling pathway is a critical mediator of oncogene-induced senescence. *Genes Dev*. 2007;21:43–8.

Supplementary Figures

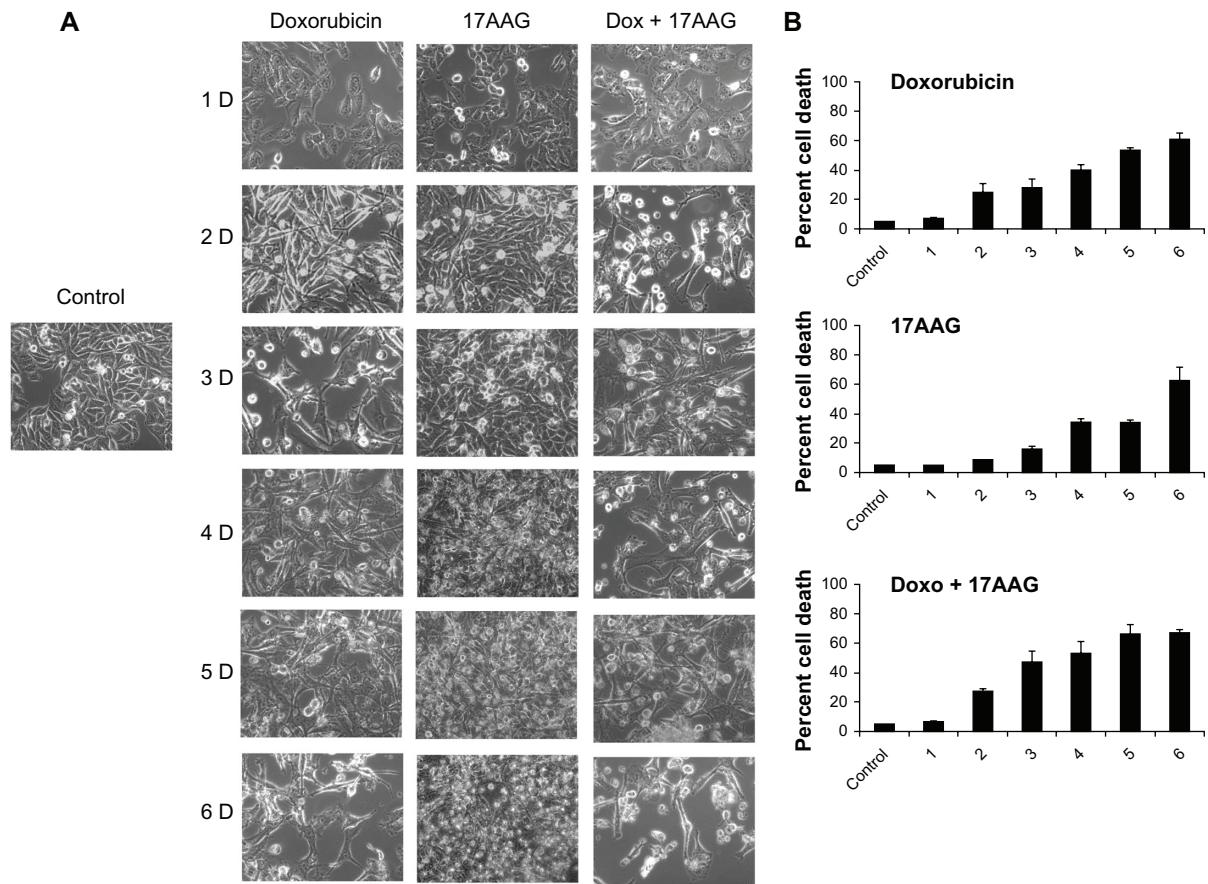


Figure S1. Effect of 17AAG, doxorubicin and their combination on cell morphology and cytotoxicity. **(A)** Cells after respective treatments were observed under microscope and phase contrast images in 10x magnification were represented. **(B)** Cells were stained with propidium iodide and the DNA content was analyzed by FACS.

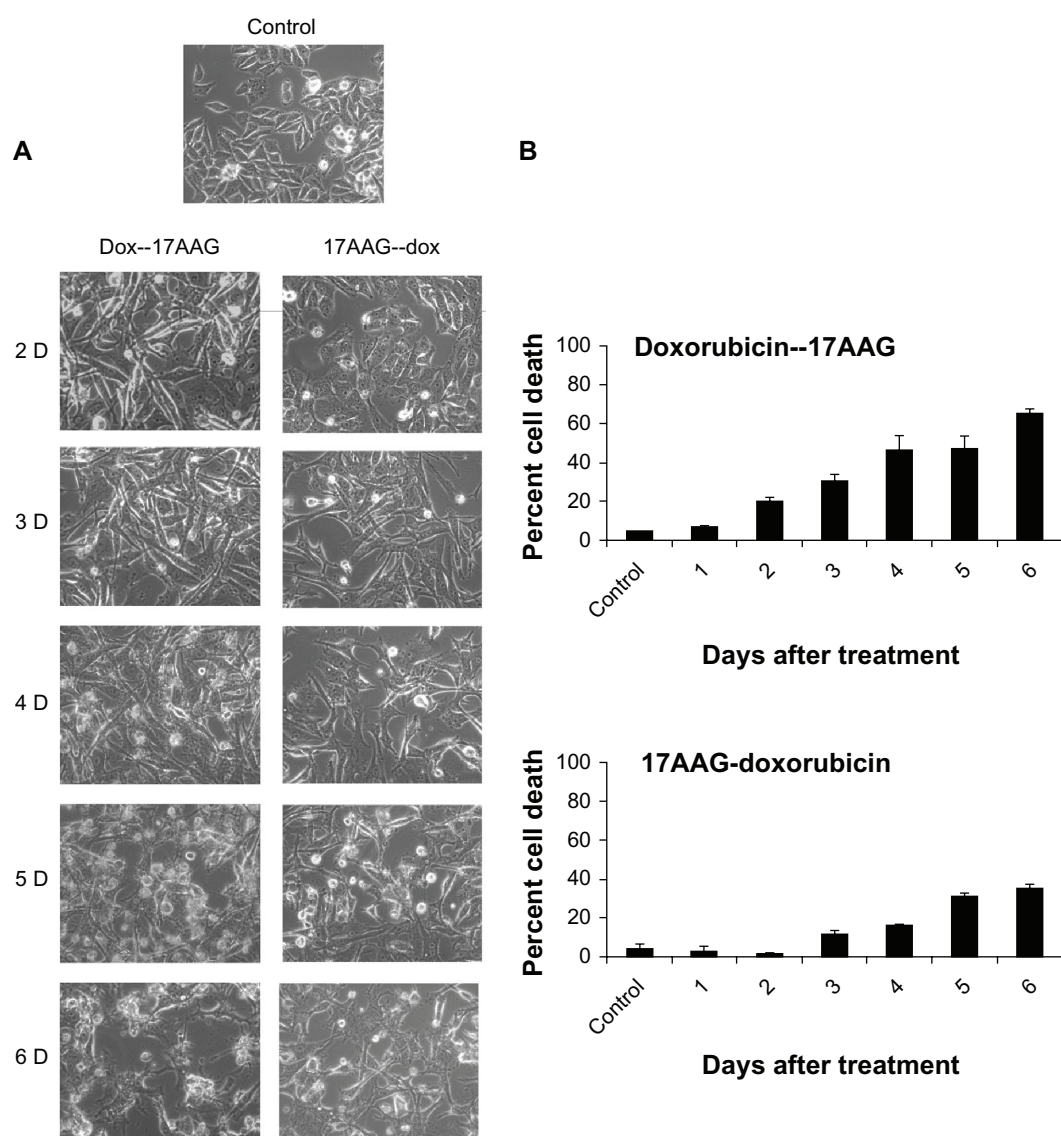


Figure S2. Effect of drugs pre-treatments on cell morphology and cytotoxicity. **(A)** Cells either treated with doxorubicin or 17AAG for 24 h followed by second drug treatment for 5-days were observed under microscope and the phase contrast images were represented. **(B)** Cells stained with propidium iodide and the DNA content was analyzed by FACS.

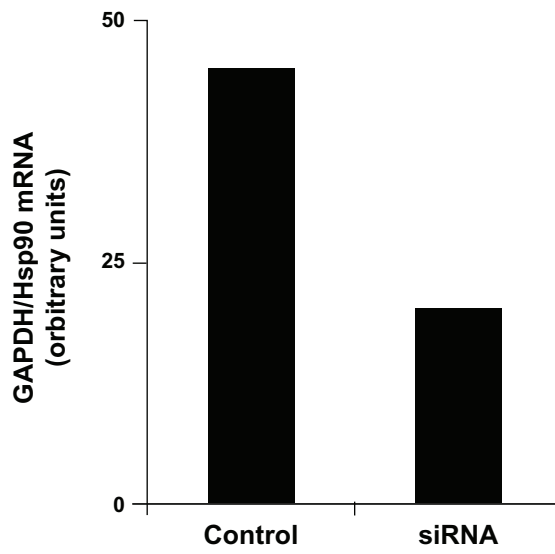


Figure S3. The RT-PCR analysis of siRNA to Hsp90 transfected cells.